Published version available: https://doi.org/10.1002/admt.201900128
Journal: Advanced Materials Technologies
Publisher: Wiley-VCH

A Magnetically Coupled Dielectric Elastomer Pump for Soft Robotics

Chongjing Cao[1,2], Xing Gao[1,3] and Andrew T. Conn[1,3]**

[1]Bristol Soft Lab, Bristol Robotics Laboratory, Bristol BS16 1QY, UK
[2]Department of Aerospace Engineering, University of Bristol, Bristol BS8 1TR, UK
[3]Department of Mechanical Engineering, University of Bristol, Bristol BS8 1TR, UK

*E-mail: a.conn@bristol.ac.uk, xing.gao@bristol.ac.uk

Conventional rigid robots are very successful at performing repeatable tasks with high precision but their application outside of controlled environments such as factories can be challenging due to complexities arising from environmental uncertainty [1]. Inspired by the embodied intelligence inherent to biological creatures, soft robots adapt to such uncertainties by deforming their bodies to interact with unstructured environments, thus reducing the sensing and computation complexity [2] [3].

Fluidic elastomer actuators in soft robotics have the advantages of low-cost, inherent compliance and multiple degree-of-freedom operations [1] [4]. A typical fluidic elastomer actuator consists of networks of expandable fluidic chambers within a highly deformable elastomer that can be driven in bending, tensile or compressive modalities and these have been utilized in manipulation [5] [6], locomotion [7] and wearable technologies [8]. Fluidic actuators are typically pneumatic and usually adopt bulky and rigid air compression systems that restrict their application in untethered mobile and wearable devices [9] [10]. The conventional setup of a single centralized air compressor with multiple distributed pneumatic actuators are further limited by the scaling of pressure losses as the air supply channels become thinner and longer. Miniature

piezoelectric, electromagnetic[11] and chemical combustion pumps [12] have the potential to decentralize the air supply to compensate for the pressure loss. However, their actuation mechanisms typically rely on rigid or inextensible components, which can introduce a hard discontinuity in soft robotic systems due to the stiffness mismatch and consequently compromise advanced behaviors such as computational morphology [13] and overcomplicate the system design.

Advancing embeddable soft pump technologies towards integrated fluidic elastomer networks requires novel solutions that move beyond the paradigm of rigid compressor technologies. Emerging soft actuators such as dielectric elastomer actuators (DEAs) possess significant shape-changing characteristics which creates opportunities for novel soft fluidic pump designs [14]. DEAs have the capacity for large actuation strains and high energy densities in a readily scalable form [15] and have been demonstrated to operate for over 400 million cycles [16]. The fundamental structure of a DEA consists of an elastic membrane sandwiched between compliant electrodes. When subjected to an electric field, the generated Maxwell stress causes the membrane to expand in-plane and compress out-of-plane. While the applied voltages of DEAs are typically high (> 1 kV), which may require encapsulation for robotic applications, recent advances in reducing the membrane thickness to only 3μm techniques using pad-printing fabrication reduced the driving voltage to 300 V [17]. Based on this actuation mechanism, many DEA-based applications were developed including grippers [18] [19], lens [20], loudspeakers [21]. Peristaltic [22] and diaphragm DEA-based pumps [23, 24, 25] have been reported. A DEA-driven fluidic micromixer demonstrated peristaltic pumping [22] but is less effective for soft robotics due to low flowrates (21.5 μL/min). DEA diaphragm pumps have shown the advantage that DE membranes can serve both as a chamber diaphragm and a compressor [23]. Diaphragm DEAs that exploit the snap-through phenomenon have demonstrated a large pumping volume and a good pressure output (~10-20 mbar, 0.84 L/min) [24], however, the large space occupation due

to snap-through limits its potential for embedded soft pump applications. A hydrostatically-coupled DEA micropump demonstrated good pumping performances (84.5 mbar, 77.4 μL/min) at its resonant oscillation [25], but it is not known how this performance will scale up to meso and macro-scales. It is notable that all current DEA pumps in the literature are hydraulic and no pneumatic pumps are available. Considering the compressibility of air, these pumps might not directly adapt to pneumatic pumping, which is a limitation for soft robotics as pneumatic operation offers reduced weight, lower viscous pumping losses and no need for a liquid container.

Here, we present an embeddable pneumatic diaphragm pump for soft robotics driven by a magnetically-coupled dielectric elastomer actuator (MCDEA [26]). The MCDEA design couples two circular DEA membranes by a magnetic repulsion (generated by centrally-located permanent magnets on each membrane) so that they protrude into a double-cone DEA configuration (**Figure 1a)**. When a voltage U is applied across the top membrane, the generated Maxwell pressure drives it upwards, which reduces the magnetic compliant coupling force and also raises the passive lower membrane (due to its elastic potential energy). By applying periodic electrical signals to each membrane 180˚ out-of-phase, the MCDEA can actuate bidirectionally to increase its total stroke. When the excitation frequency matches the resonant frequency of the DEA, the stroke/power output can be greatly magnified [19] [26] [28].

A typical dynamic response of the MCDEA with silicone elastomer membranes is shown in **Figure 1b** with periodic displacements in one cycle shown on the right side. Due to the compliant coupling of the two DEA membranes by magnetic repulsion, the strokes of the two membranes (d_1, d_2, as illustrated in blue and red) are not necessarily the same and the distance between the two biasing magnets, s, can significantly vary within one cycle (green dash curves). The MCDEA exhibits a linear frequency response in a wide range of excitation frequencies with a super-harmonic occuring only during the first peak. The only mode shape observed for

each membrane across all tested frequencies is axisymmetric translation along the vertical axis. The dynamic performance of the MCDEA was also investigated against different voltage amplitudes, U_{peak} (**Figure 1c**), and different spacer heights, h (**Figure 1d**), with power consumption available in supplementary **Figure S1**. By increasing U_{peak}, both the stroke and the power consumption increased. While, in this work, a maximum voltage of 4515 V (nominal electric field of about 70 V/μm) was adopted in order to minimize the failure rate of the DEA. Comparing the DEA performance against the excitation frequency, three local minimums of the power consumption can be found at the frequencies where the three stroke peaks occur, demonstrating the clear advantage of resonant actuation to magnify the output with an increased efficiency.

The MCDEA diaphragm pump design is illustrated in **Figure 2a**. The bottom membrane of the MCDEA is attached to the pump chamber frame and serves as the pump diaphragm. The air chamber was designed to match the conical geometry of the DEA membrane to maximise the actuator stroke (**Figure S2b**). The top DEA membrane is separated from the bottom membrane with the distance, h. Passive check valves (12.5 mbar breaking pressure) are connected to the inlet and outlet of the pump, allowing air flow into the chamber when the chamber volume expands (filling stage) and pumping air out when the chamber compresses (venting stage) (**Figure 2b**). Since the DEA membranes have minimal radial stretch, the MCDEA pump design can be almost entirely soft and flexible, as shown in **Figure S3**. While the passive check valves are rigid in the current pump design, these are available with maximum dimensions of less than 10 mm[27] which can minimise their impact.

The performance of the pump with various h and U_{peak} = 4515 V was characterized by inflating a hyperelastic balloon chamber, and the measured flowrate and output pressure (inside the balloon) are shown in **Figure 2c-e** (experimental setup shown in supplementary **Figure S4**). For all values of h, the frequency response for both output pressure and flowrate show distinct

peaks. Taking the smallest *h* of 1.8 mm as an example, both the maximum output pressure and the maximum flowrate increases to peaks of 24.3 mbar and 0.92 standard litres per minute (SLPM), respectively, at 77 Hz (supplementary **Figure S5a**). Thanks to the resonant actuation of the MCDEA, the stroke reaches the peak at 77 Hz where the pump achieves its maximum output and this is also where power consumption drops to a global minimum of 41.5 mW at 79 Hz, which significantly increases the efficiency (supplementary **Figure S5b**).

As the two membranes are separated further (increase of *h*), the magnetic repulsion force reduces and the lower DEA membrane tension results in a reduced elastic stiffness and resonant frequency (**Figure 1d**). Consequently, the frequency at which the output pressure and peak flowrate occurs at reduces with increased membrane spacing, *h*. The peak flowrate of the pump also reduces with increasing *h* (**Figure 2c**). While the maximum output pressure also increases with *h*, it does so only up to h = 5.4 mm, where it has a peak of 30.2 mbar (total pumping pressure 42.7 mbar). As *h* increases further, the maximum output pressure reduces which is likely due to increased compression of the MCDEA's compliant coupling, since the magnetic repulsion force reduces with *h*. It also can be noticed in **Figure 2d** that as *h* increases, the peak becomes sharper. If a specific minimum pressure output of, say, 10 mbar is required for potential soft robotic applications, then it can be concluded that a pump with a shorter *h* value can have a larger bandwidth where the pressure output is greater than 10 mbar (as indicated in black dash line in **Figure 2d**). **Figure 2e** shows the relationship between flowrate and output pressure during a pumping at the frequencies where the peak pressures occur, which is approximately linear for this pump design. Both output pressure and flowrate increase monitonically with increasing voltage amplitude at resonance (**Figure 2f**).

Several demonstrations of the MCDEA pump for soft robotics are shown in **Figure 3**. In **Figure 3a**, the MCDEA pump was used to inflate a silicone elastomer balloon with a diameter of 60 mm. Despite having a much larger size than the pump (diameter of 30 mm), a relative fast

response was achieved e.g. 18.5 mbar within 4 secs (supplementary **Video S1**). A two-finger soft gripper was designed (shown in supplementary **Figure S6**), which was directly connected to the outlet of the pump and an object up to 68g could be firmly grasped (**Figure 3b** and supplementary **Video S2**). The MCDEA pump can also be employed in a suction mode, as shown in **Figure 3c** and supplementary **Video S3** where a 15g mass is lifted. Arrays of miniature suction cups could potentially mimic the octopus tentacle [29]. Thanks to the contactless coupling between membranes by magnetic repulsion, the MCDEA pump can work in an electrically isolated mode, where the pump chamber interfaces with a passive membrane and the active DEA membrane is separated (supplementary **Figure S7** and **Video S4**). This mode would be beneficial when the chamber needs to be embedded within a galvanically isolated condition e.g. biomedical applications.

A key distinction of the MCDEA compared to conventional rigidly-coupled double cone DEAs [30] is that the magnetic coupling is compliant and the distance between two membranes is not fixed. To demonstrate the advantage of compliant coupling for diaphragm pumping, the pumping performance of an equivalent rigidly-coupled double cone DEA was briefly characterized (supplementary **Figure S8**). No resonant peak was observed with the rigidly-coupled DEA pump and the maximum pressure generated was an order of magnitude less than the peak pressure from the MCDEA pump at resonance (**Figure 2d**). Because the lower DEA membrane acts as the chamber diaphragm and directly compresses air, the stroke of the rigidly-coupled membranes are damped, which results in a significant reduction in its output. The damping of the rigidly-coupled DEA pump's oscillatory response is compounded by the dynamical discontinuity introduced by the check valves, which open and close at the cracking pressure. The compliant coupling in the MCDEA pump adds an additional degree-of-freedom that helps decouple the oscillatory response from this damping and hence it is shown to still oscillate freely with a high stroke to maximize pumping output. This is demonstrated in **Figure**

S9, where the actuation stroke of the top membrane in the MCDEA pump increases with pumping pressure, P_{out}, before saturating above 30 mbar.

By characterizing the pumping performance against the actuation voltage amplitude, excitation frequency and DEA geometry, it can be concluded that this pump design can be easily customized to meet different demands for various applications. For example, output pressure and flowrate can be tuned by adjusting either the actuation voltage amplitude or frequency via a control signal. If a maximum flowrate or pressure is required, the height of the spacers between two membranes can be adjusted (h = 1.8 mm for maximum flow rate and h = 5.4 mm for maximum pressure for the current prototype).

The passive check valves may have some minimal leakage under back-pressure so there is potential to improve the pumping performance by replacing them with miniature active valves capable of crisp opening and closing. There is potentially also scope to optimize the chamber geometry further, but such improvements may be restricted by the rated power output of the high voltage power supply since its load increases as the DEA membranes stack up with multiplied capacitance and resistance. Future work will explore how a fully soft embodiment of the pump performs during externally applied deformations (such as those shown in **Figure S3(b)**).

In this work, the first DEA-driven pneumatic pump was developed. The magnetically coupled double cone DEA demonstrated an excellent dynamic performance with a peak stroke at resonance of over 800% of that at low frequencies. The proposed pump design also exhibited a peak pressure output and flowrate at the resonance of the driving DEA. The current prototype demonstrated a maximum pressure output of 30.5 mbar and a flowrate of 0.9 SLPM at a relatively low power consumption of 40 mW. The performance of this pneumatic pump design was then demonstrated by integrating it with soft robotic demonstrators, including a soft gripper

and a suction cup. In conclusion, this novel DEA driven pneumatic pump offers an alternative for efficient and high-performance soft pumps in future of soft robotics applications.

Experimental Section

Fabrication of MCDEA pump: The detailed assembly is shown in supplementary **Figure S2**. Silicone elastomer (Elastosil, 100 μm thickness, Wacker Chemie AG) was stretched biaxially by 1.2 × 1.2, then bonded to an acrylic frame with an inner diameter of 30 mm by silicone transfer tape (ARclear 93495, Adhesives Research). This biaxial pre-stretch was selected after our previous study of the MCDEA design [26], which showed that a relatively low applied pre-stretch of 1.2 × 1.2 generates a higher force-stroke output with 100 μm Elastosil membranes. Four layers of membranes were stacked together on each side of the MCDEA and 15 mm diameter × 1 mm thick disc magnets (3×1.1 kg pull force, First4Magnets) were attached to the centre utilizing the transfer tape (**Figure S2b**). The selected ratio of magnet to membrane diameters of 0.375 has been shown to ensure stable MCDEA operation across a wide range of excitation frequencies [26]. Conductive carbon grease (MG Chemicals) was hand-brushed on the membrane as the compliant electrodes. The top and bottom membrane stacks were separated by Nylon spacers. The main body of the pump was fabricated by 3D printing (PLA) with dimensions sown in **Figure S2c**. Nylon miniature check valves (12.5 mbar breaking pressure, NO.7005, Cole-Parmer) were connected to the inlet and outlet. The MCDEA was attached to the pump frame via M3 bolts and fasteners. The soft version of the pump chamber shown in **Figure S3** was fabricated with flexible DEA frames (0.2 mm PVC sheet) and a 3D printed chamber (Tango Black, Eden 350V printer, Objet Geometries). The rigidly-coupled DEA in **Figure S8** was fabricated with the same approach as the MCDEA except that the top and bottom membrane stacks were coupled by a 15 mm spacer.

Characterisation of dynamic response of MCDEA: The DEA support frame was fixed to the testing rig while allowing the centre of the membranes to move freely. Two alternating

sinusoidal waves $U_1 = U_{peak} \sin(2\pi f t)$ and $U_2 = U_{peak} \sin(2\pi f t + \pi)$ were applied to the two membrane stacks respectively via two high-voltage amplifiers (Ultravolt, 5HC23-BP1). The power consumption of the DEA was estimated based on the measured actuation voltage and current flow into the DEA (measured from the high-voltage amplifier's feedback signal). The displacements of the two membranes were measured by two laser displacement sensors (LK-G152 and LKGD500, Keyence). All experiments were controlled by MATLAB (MathWorks) and all data was collected by a DAQ device (National Instruments, BNC-2111) at a sampling frequency of 20,000 Hz.

Characterisation of pumping performance of MCDEA pump: The experimental setup for the MCDEA diaphragm pump's characterization is shown in supplementary **Figure S4**. The pump was actuated to pump into a bespoke balloon (60 mm in diameter, 100 um thickness Elastosil membrane) where the pressure in the balloon was measured using a pressure sensor (SSCSNBN015PDAA5, Honeywell) and the inlet flowrate was measured by a flowrate sensor (AWM5101VN Mass Air Flow Sensor, Honeywell).

Supporting Information

Supporting Information is available from the Wiley Online Library or from the author. The underlying data is available from the Research Data Repository of the University of Bristol at https://doi.org/10.5523/bris.3tyiulqwo5czp2mg5dmkkcxd22.

Acknowledgements

C. Cao and X. Gao contributed equally. C. Cao appreciates the support from the EPSRC Centre for Doctoral Training in Future Autonomous and Robotic Systems (FARSCOPE) at the Bristol Robotics Laboratory. A. Conn and X. Gao appreciate the support by EPSRC grant EP/P025846/1.

References

[1] D. Rus, M. T. Tolley, *Nature* 2015, 521, 467.
[2] S. I. Rich, R. J. Wood, C. Majidi, *Nature Electronics* 2018, 1, 102.
[3] C. Laschi, B. Mazzolai, M. Cianchetti, Sci. Robot. 2016, 1, eaah3690.
[4] C. Laschi, M. Cianchetti, *Frontiers in Bioengineering and Biotechnology* 2014, 2, 3.

[5] M. Cianchetti, T. Ranzani, G. Gerboni, T. Nanayakkara, K. Althoefer, P. Dasgupta, A. Menciassi, *Soft Robotics* 2014, 1, 122.
[6] S. Shian, K. Bertoldi, D. R. Clarke, Advanced Materials 2015, 27, 6814.
[7] R. F. Shepherd, F. Ilievski, W. Choi, S. A. Morin, A. A. Stokes, A. D. Mazzeo, X. Chen, M. Wang, G. M. Whitesides, *PNAS* 2011, 108, 20400.
[8] P. Polygerinos, Z. Wang, K. C. Galloway, R. J. Wood, C. J. Walsh, *Robotics and Autonomous Systems* 2015, 73, 135.
[9] A. A. Stokes, R. F. Shepherd, S. A. Morin, F. Ilievski, G. M. Whitesides, *Soft Robotics* 2014, 1, 70.
[10] M. T. Tolley, R. F. Shepherd, B. Mosadegh, K. C. Galloway, M. Wehner, M. Karpelson, R. J. Wood, G. M. Whitesides, *Soft Robotics* 2014, 1, 213.
[11] D. J. Laser, J. G. Santiago, *Journal of Micromechanics and Microengineering* 2004, 14, R35.
[12] C. Stergiopulos, D. Vogt, M. T. Tolley, M. Wehner, J. Barber, G. M. Whitesides, R. J. Wood, "A soft combustion-driven pump for soft robots", presented at *ASME 2014 Conference on Smart Materials, Adaptive Structures and Intelligent Systems*, 2014.
[13] H. Hauser, A. J. Ijspeert, R. M. Füchslin, R. Pfeifer, W. Maass, *Biological Cybernetics* 2011, 105, 355.
[14] Y. Bar-Cohen, *Electroactive polymer (EAP) actuators as artificial muscles: reality, potential, and challenges*, Vol. 5, 2004.
[15] R. Pelrine, R. Kornbluh, Q. Pei, J. Joseph, *Science* 2000, 287, 836.
[16] L. Maffli, S. Rosset, M. Ghilardi, F. Carpi , H. Shea, *Advanced Functional Materials* 2015, 25 , 1656.
[17] A. Poulin, S. Rosset, H.R. Shea, "Fully printed 3 microns thick dielectric elastomer actuator", presented at *Proc. SPIE 9798, Electroactive Polymer Actuators and Devices (EAPAD) 2016*, 97980L.
[18] J. Shintake, S. Rosset, B. Schubert, D. Floreano, H. Shea, *Advanced Materials* 2016, 28, 231.
[19] X. Gao, C. Cao, J. Guo, A. Conn, *Advanced Materials Technologies*, 1800378.
[20] F. Carpi, G. Frediani, S. Turco, D. De Rossi, *Advanced Functional Materials* 2011, 21, 4152.
[21] C. Keplinger, J.-Y. Sun, C. C. Foo, P. Rothemund, G. M. Whitesides, Z. Suo, *Science* 2013, 341, 984.
[22] S. Solano-Arana, F. Klug, H. Mößinger, F. Förster-Zügel, H. F. Schlaak, *Smart Materials and Structures* 2018, 27, 074008.
[23] L. Maffli, S. Rosset, H. Shea, *Smart Materials and Structures* 2013, 22, 104013.
[24] Z. Li, Y. Wang, C. C. Foo, H. Godaba, J. Zhu, C. H. Yap, *Journal of Applied Physics* 2017, 122, 084503;
[25] J. J. Loverich, I. Kanno, H. Kotera, Lab on a Chip 2006, 6, 1147.
[26] C. Cao, X. Gao, A. Conn, *Applied Physics Letters* 2019, 114, 011904.
[27] Smart Products USA Inc., Model #101 1/8" check valve, http://www.smartproducts.com/check_valves_series_100_cartridge_specialty.php, accessed: March, 2019.
[28] C. Cao, S. Burgess, A. T. Conn, "Flapping at resonance: Realization of an electroactive elastic thorax", presented at *2018 IEEE International Conference on Soft Robotics (RoboSoft)*, 2018.
[29] S. Sareh, K. Althoefer, M. Li, Y. Noh, F. Tramacere, P. Sareh, B. Mazzolai, M. Kovac, J*ournal of the Royal Society: Interface* 2017, 14, 135.
[30] A. T. Conn, J. Rossiter, *Smart Materials and Structures* 2012, 21, 035012.

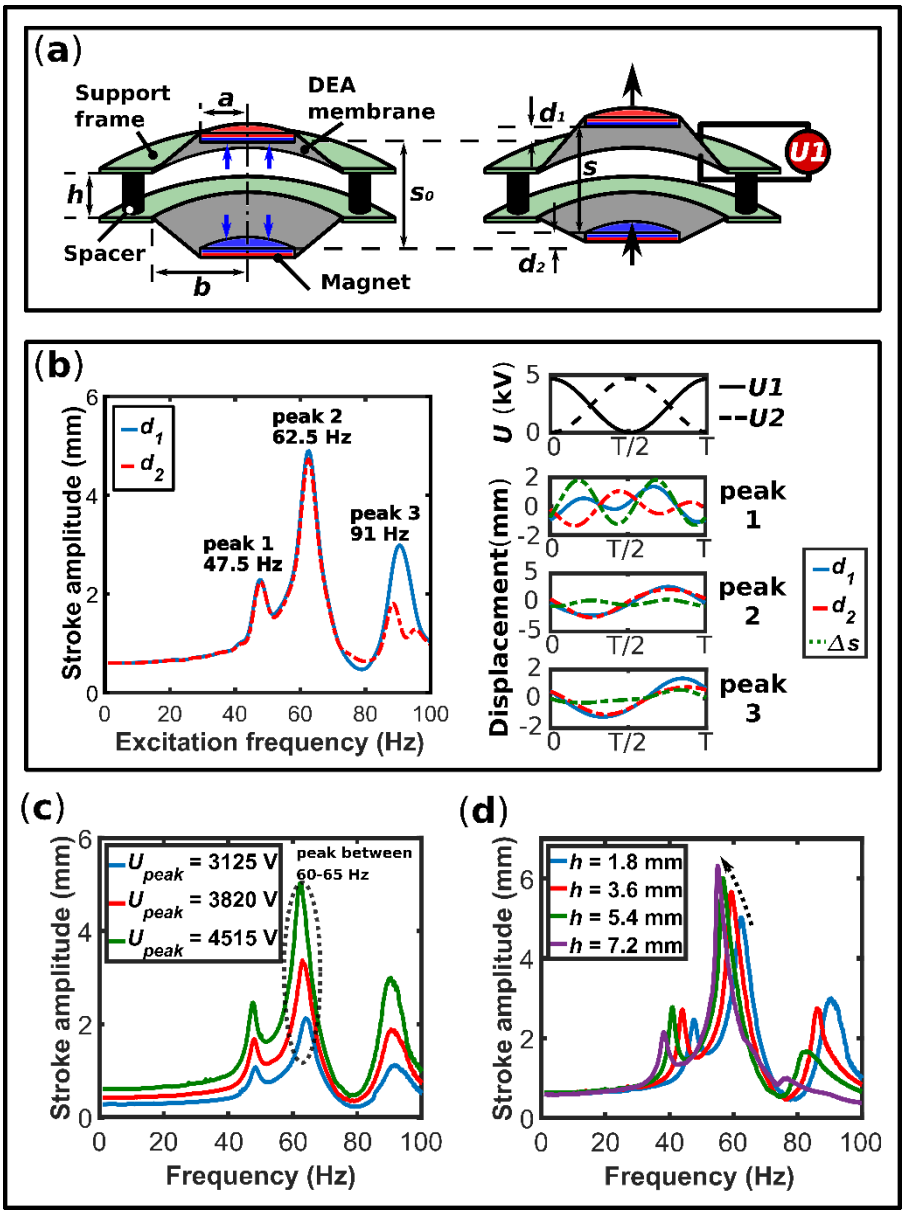

Figure 1. (a) Schematic diagram of MCDEA shows the magnets (radius a) are attached to the center of the DE membranes (radius b); the same pole of the two permanent magnets are facing each other to bias the two DE membranes with a distance, s_0, by magnetic repulsion; the support frame of the two DEA membranes are separated by spacers with a height, h. (b) Typical dynamic responses of frequency swept from 1 to 100 Hz with spacer height h = 1.8 mm and actuation voltage amplitude U_{peak} = 4515 V are shown on the left, where it can be observed that the stroke d_1 at second peak is the highest with an amplitude 816% of that at low frequencies (< 10 Hz); The periodic responses in the time domain of strokes d_1 and d_2 and the maximum change of s per cycle, Δs, are shown on the right-hand side of (b). Dynamic responses at various (c) actuation voltage amplitudes and (d) spacer heights.

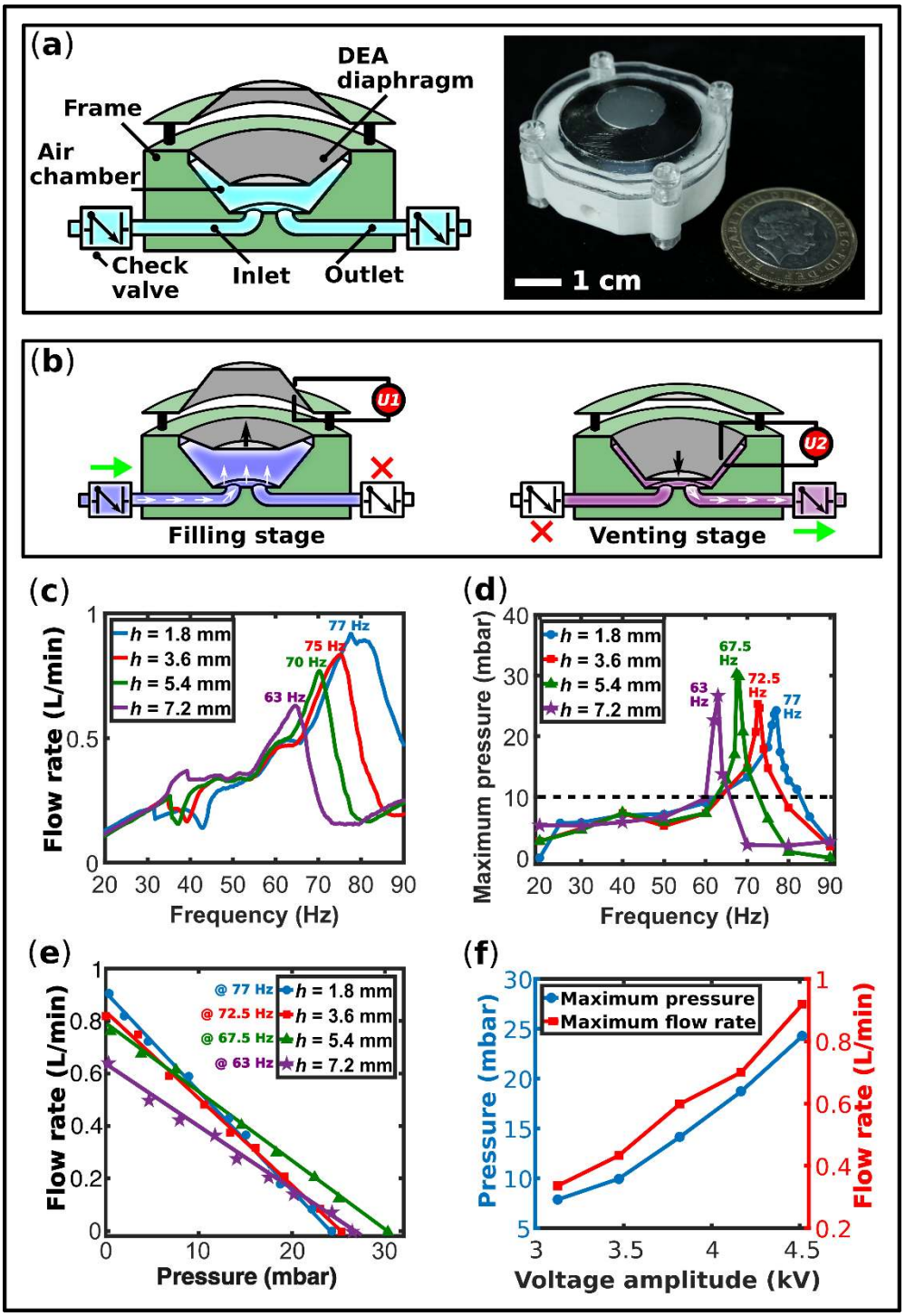

Figure 2. (a) Structure of the MCDEA pump. MCDEA serves as both the pump diaphragm and the compressor. (b) Working mechanism of the MCDEA pump. When voltage applied on upper membrane, MCDEA moves upwards suck air in and the pump works in filling stage; when voltage applied on lower membrane, MCDEA moves downwards to compress the air out and the pump works in venting stage. Pumping performances in terms of (c) flowrate and (d) output pressure as a function of frequency of excited voltage at various spacer height, *h*. (e) The MCDEA pump demonstrates approximately linear flowrate-pressure behavior. (f) Dependence of pressure and flowrate with voltage amplitude (h = 1.8 mm).

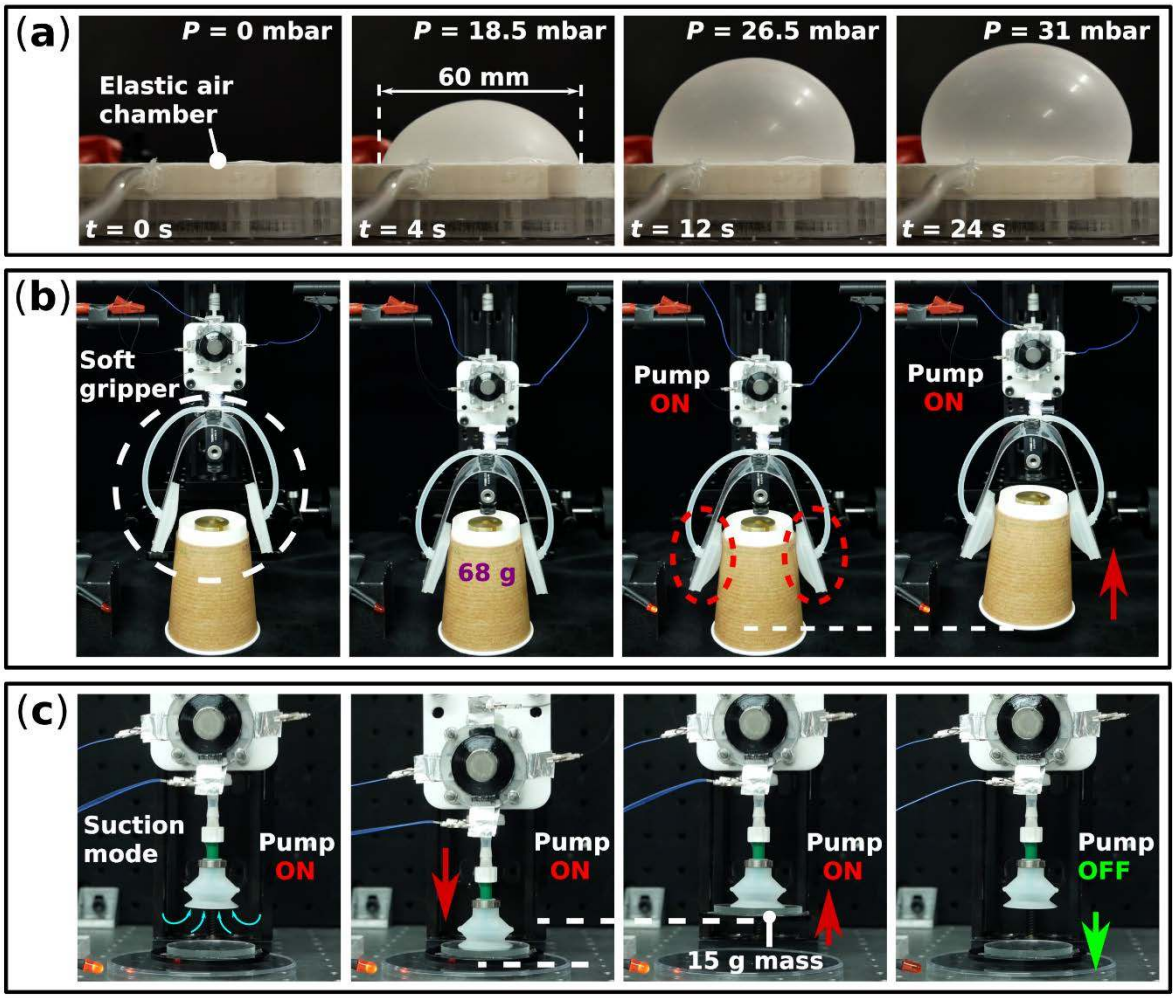

Figure 3. Demonstrations of potential applications for soft robotics. (a) Inflation of elastic balloon chamber. The MCDEA pump can function in both (b) inflation mode (soft gripper) and (c) suction mode (suction cup).

Supporting Information

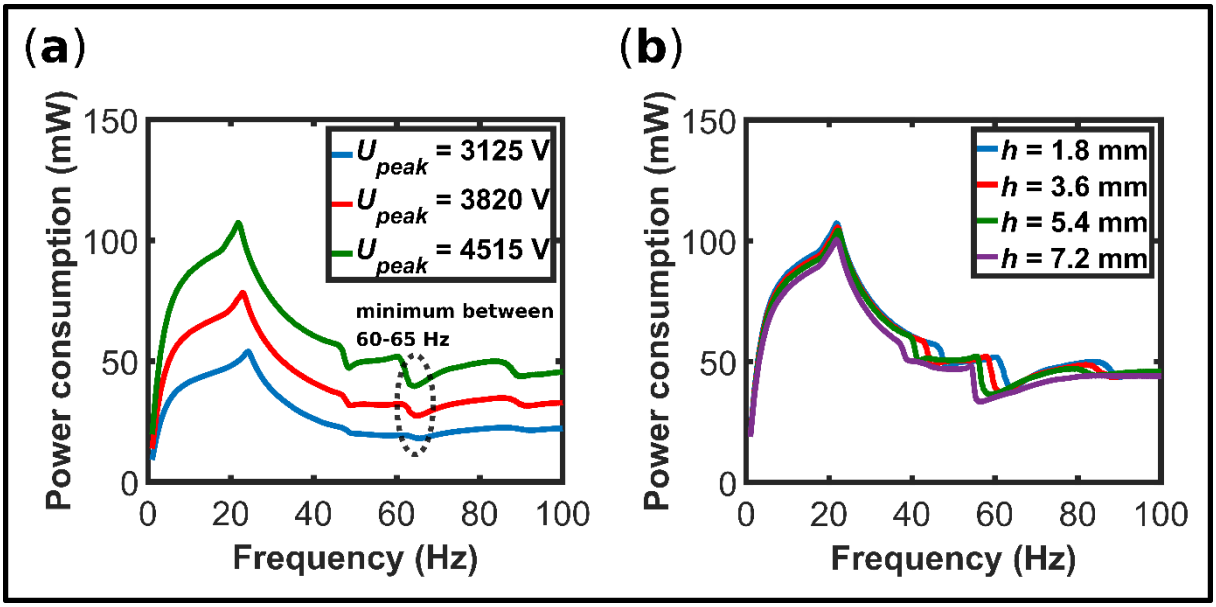

Figure S1. Power consumption of the MCDEA as a function of applied frequency at various (a) voltage amplitudes and (b) spacer heights (with U_{peak} = 4515 V).

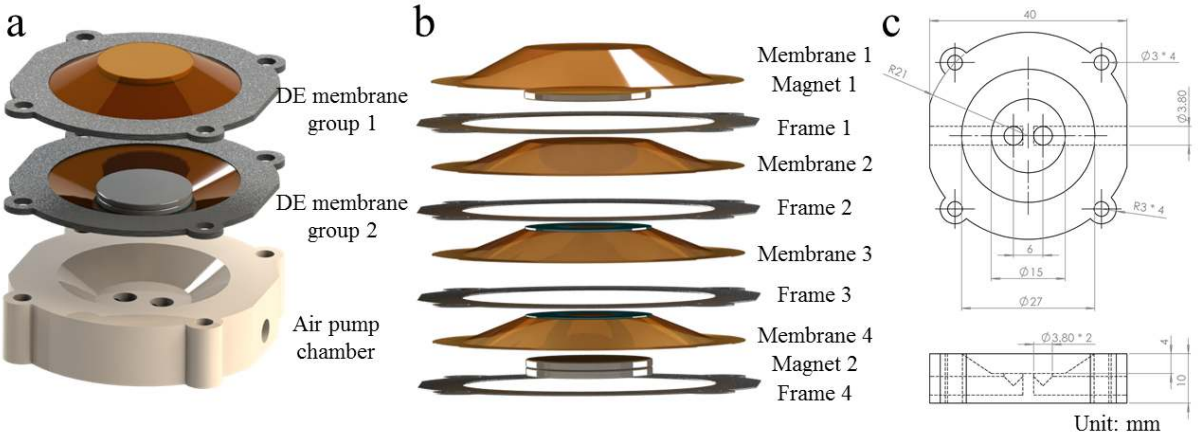

Figure S2. Assembly of (a) the MCDEA pump and (b) DE membranes and magnets. (c) Dimensions of the 3D printed pump chamber.

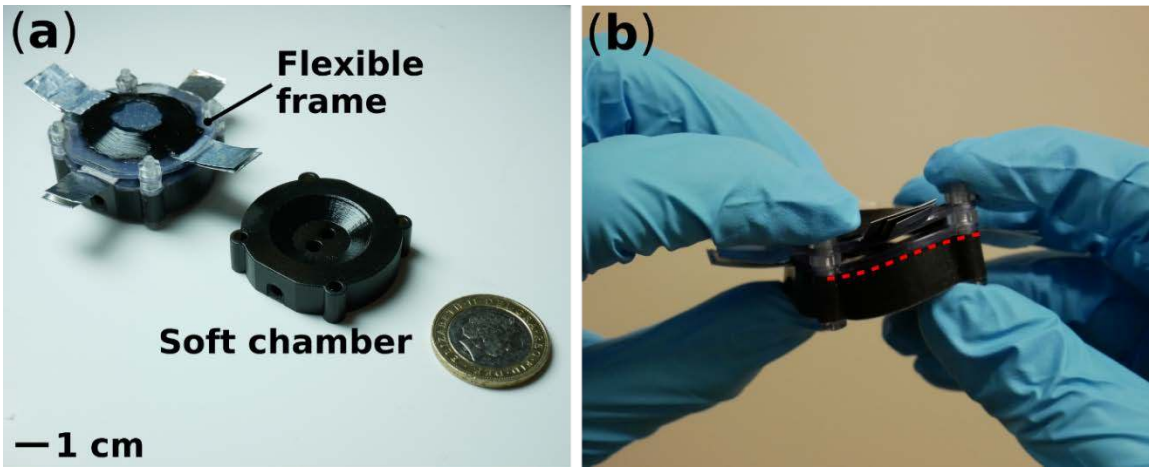

Figure S3. Soft MCDEA pump prototype with (a) flexible membrane frame (0.2 mm PVC sheet) and 3D printed soft chamber (Tango Black, Eden 350V printer, Objet Geometries), which (b) exhibits flexibility and compliance.

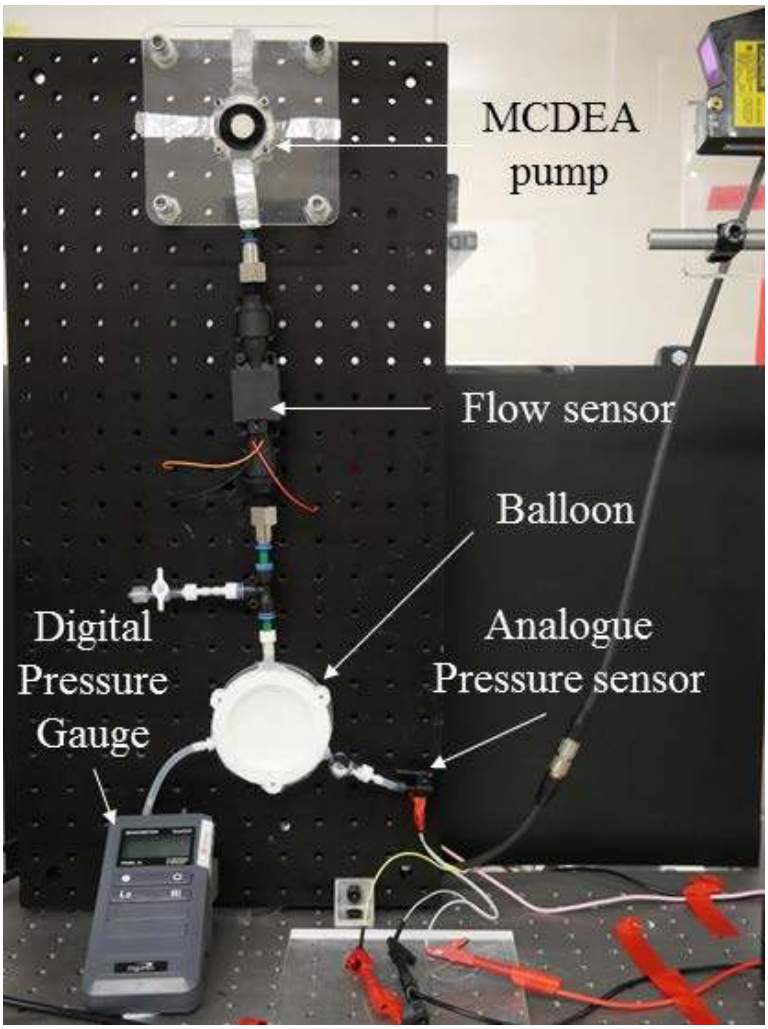

Figure S4. Experimental setup for characterization of pumping performances of the MCDEA pump. The digital pressure gauge was used to ensure the data from analogue pressure sensor is reliable.

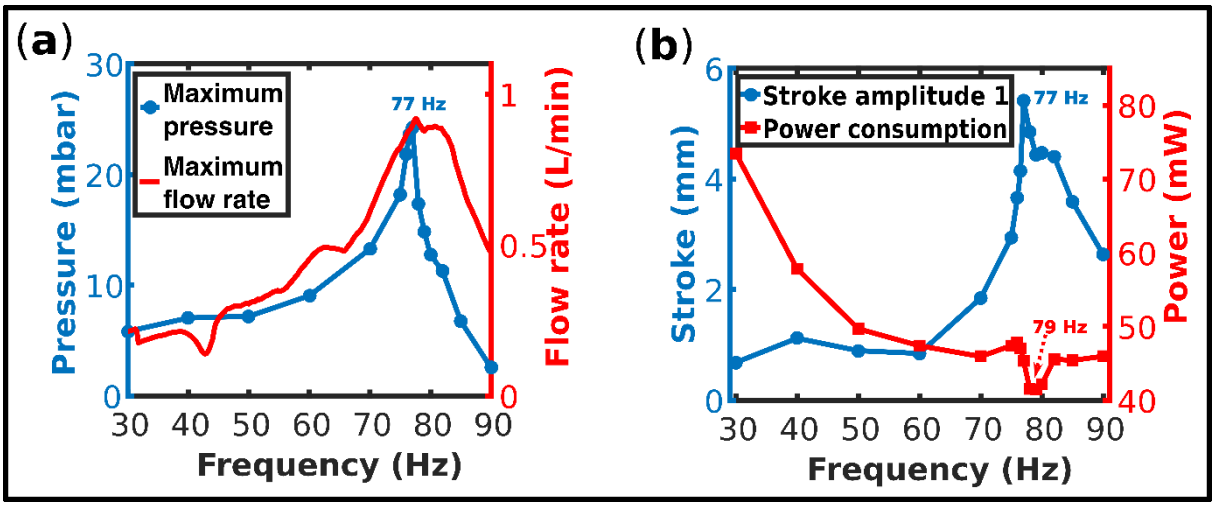

Figure S5. (a) Maximum output pressure and flowrate and (b) DEA stroke and power consumption as a function of frequency with h = 1.8 mm (in both cases, U_{peak} = 4515 V). The maximum pressure, flowrate and stroke occurred at 77 Hz which is believed to be resonant frequency, and the minimum power consumption at 79 Hz (note that power values do not include losses in the high-voltage amplifier).

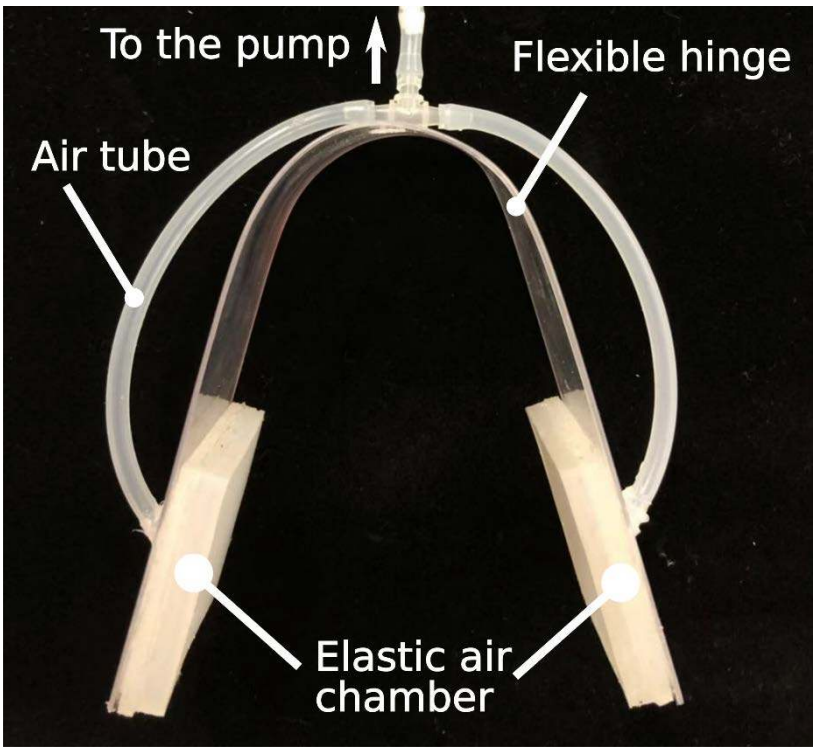

Figure S6. The simplified two-finger soft gripper used in this study consists of two elastic air chambers (Ecoflex 00-30, Smooth-On) fixed on a flexible hinge (1 mm thick acrylic).

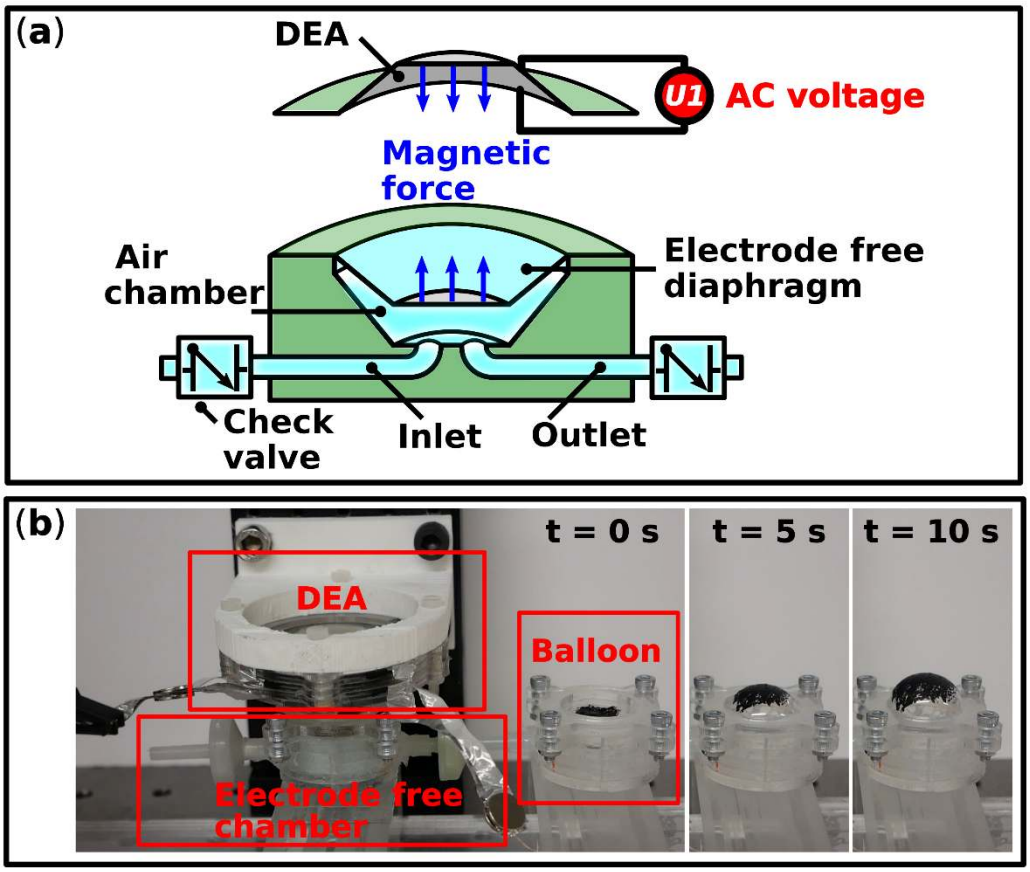

Figure S7. (a) Via compliant coupling of magnetic repulsion, the MCDEA pump can be separated into two parts – a pump chamber with passive diaphragm and an active DEA. (b) This allows an electrically-isolated mode.

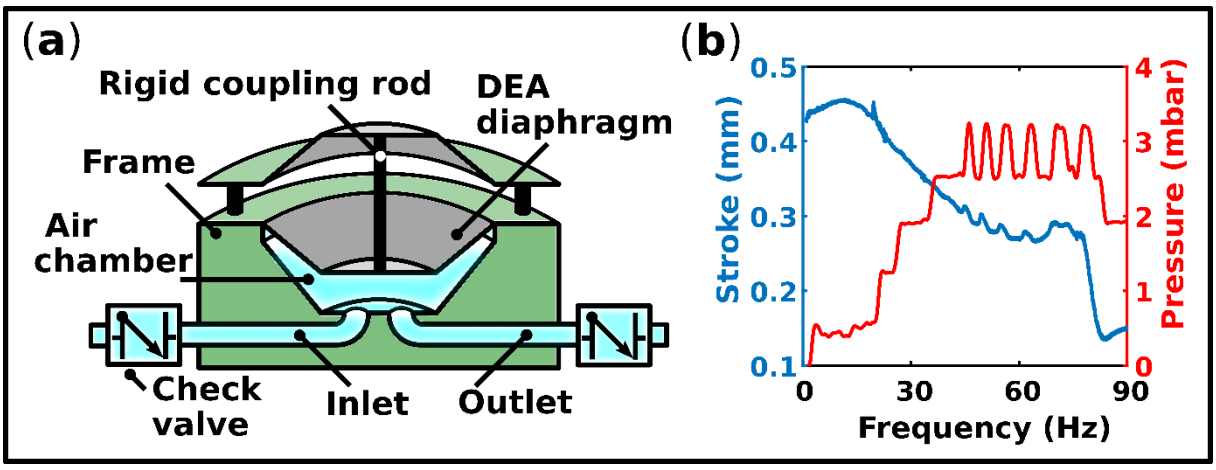

Figure S8. (a) A rigidly-coupled double cone DEA pump. (b) Due to the damping of both DEA membranes, the stroke of the DEA is greatly reduced and no resonant behavior is observed, resulting in dramatical reduction in its pumping performances.

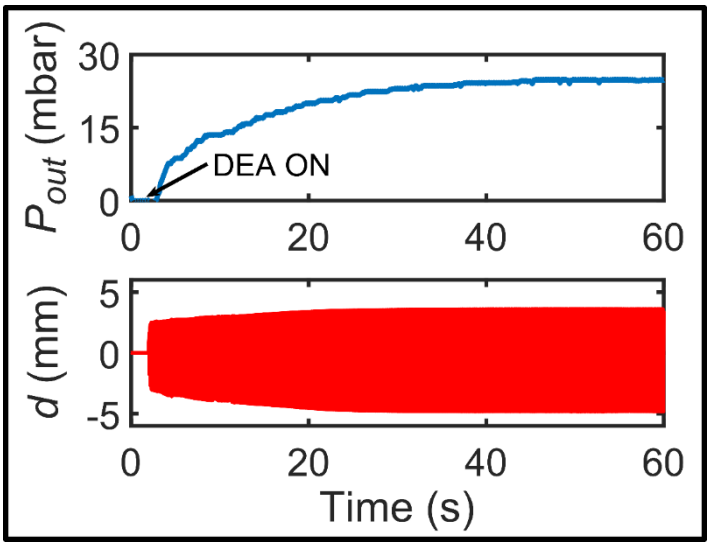

Figure S9. The relationship between pumping pressure, $P_{out,}$ and actuation stroke, d, of the top membrane in the MCDEA pump shows that d increases with P_{pout} before saturating above 30 mbar (driven with U_{peak} = 4515 V).